Subdivision and microtexture development in f.c.c. grains during plane strain compression

M. Arul Kumar[a], Sivasambu Mahesh[a,b,*]

[a] *Department of Mechanical Engineering,*
[b] *Department of Aerospace Engineering,*
Indian Institute of Technology, Kanpur 208016. India.

Abstract

Grains in f.c.c. polycrystals deform non-uniformly even under imposed homogeneous deformation and subdivide into domains of different lattice orientations. Intense non-uniformity of grain deformation produces substructural features called deformation bands and shear bands, wherein large deviations from the average lattice orientation and/or slip localization occur. Using a model of grain banding, subdivision of pure copper grains initially oriented along the α, β and τ fibers of the copper-type f.c.c. rolling texture under imposed homogeneous plane strain deformation is characterized. The microtexture developed in grains of these lattice orientations is predicted. The predicted banding response and microtexture quantitatively agree with experimental observations reported in the literature.

Keywords: crystal plasticity, shear band, deformation band, dislocation boundary, rolling texture

1. Introduction

During plastic deformation, grains of coarse-grained f.c.c. polycrystals may sub-divide into highly misoriented domains, called bands. This process, termed banding, is classified into two types: shear banding (Wagner et al., 1995; Jasienski et al., 1996) and deformation banding (Heye and Sattler, 1971; Lee and Dug-

*Corresponding author
Email address: smahesh@iitk.ac.in (Sivasambu Mahesh)

gan, 1993; Hughes and Hansen, 1997; Liu and Hansen, 1998; Kulkarni et al., 1998; Wu et al., 2011). In shear banded grains, long and narrow regions of intense slip localization called shear bands, run through the grain matrix. Considerable lattice misorientation develops between the shear bands and matrix (Wagner et al., 1995; Jasienski et al., 1996). In deformation banded grains, on the other hand, highly misoriented bands of approximately equal volume (Lee and Duggan, 1993) develop, but intense slip localization does not occur. Following the usage followed by Lee and Duggan (1993) and Wagner et al. (1995), the term 'banding' presently excludes grain subdivision into slightly misoriented volumes such as cells, cell-blocks or microbands (Bay et al., 1989).

Both texture evolution and banding, which occur during plastic deformation, determine the plastic anisotropy of the deformed material. Texture evolution is well-characterized experimentally and well-predicted by models that assume homogeneous grain deformation for a variety of materials and deformation paths as detailed in Kocks et al. (1998) and references therein; the same cannot be said of banding. Banding has been experimentally studied in ideally oriented single crystals, e.g., Wagner et al. (1995); Liu and Hansen (1998); Paul et al. (2002, 2009, 2010) and in certain grains of polycrystals, e.g., Lee and Duggan (1993); Hughes and Hansen (1997); Kulkarni et al. (1998); Paul and Driver (2008); Wu et al. (2011). It is recognized that lattice orientation largely determines the occurrence and type of banding (Hughes and Hansen, 1997; Wu et al., 2011). However, a systematic experimental characterization of the lattice orientation dependence of banding is presently prohibitively tedious and not presently available. Such a characterization may be obtained from banding models.

Deformation banding is driven by the tendency to minimize the plastic power during plastic deformation. This principle, first recognized by Chin and Wonsiewicz (1969), has since been extended and phrased in terms of plastic work (Lee and Duggan, 1993; Lee et al., 1993) and free energy (Kuhlmann-Wilsdorf, 1999) minimization. Shear banding was explained by Van Houtte et al. (1979); Dillamore et al. (1979); Asaro (1979) as resulting from load instability caused by geometric and vertex softening. A more recent model (Mahesh, 2006) simul-

taneously explains both deformation banding and shear banding as unstable growth of small random lattice orientation perturbations during plastic power minimizing grain deformation.

In recent years, the crystal plasticity finite element method (CPFEM) (Roters et al., 2010) has been extensively used to model deformation banding (Rezvanian et al., 2006; Si et al., 2008; Kanjarla et al., 2010) and shear banding (Anand and Kalidindi, 1993; Kuroda and Tvergaard, 2007) in single crystals and grains. The underlying variational principle of CPFEM ensures minimization of the incremental plastic work over each time step. Also, material compatibility is automatic because element deformations are interpolated from nodal displacements.

In CPFEM simulations, deformation inhomogeneity and banding may emerge spontaneously during simulated model deformation, obviating complex nonlinear constrained optimization procedures as in Mahesh (2006). However, the number of degrees of freedom required to capture banding in a CPFEM model is much larger than that in the models of Chin and Wonsiewicz (1969); Lee and Duggan (1993); Lee et al. (1993); Kuhlmann-Wilsdorf (1999); Van Houtte et al. (1979); Dillamore et al. (1979); Asaro (1979) and Mahesh (2006). CPFEM calculations, therefore, typically involve several orders of magnitude more computational effort than that required by these models.

A 'stack of domains' model of a grain, capable of capturing inhomogeneous deformation and banding with far fewer degrees of freedom than CPFEM models was recently developed by Arul Kumar and Mahesh (2012). In this model, banding may emerge spontaneously during simulated model grain deformation, as in CPFEM. Continuity between each domain and its two neighbors is enforced, as between adjacent elements in CPFEM. However, in contradistinction to CPFEM model elements, the shape of the domains in the model of Arul Kumar and Mahesh (2012) resembles experimentally observed lath-shaped bands that run across the grain (Lee and Duggan, 1993; Wagner et al., 1995). Also, model domains are assumed to deform homogeneously. Further, 'stack of domains' model boundaries may be mobile relative to the crystalline material, in

accord with experimental observations (Wagner et al., 1995; Jasienski et al., 1996). This contrasts with the immobility of CPFEM element boundaries. On account of these assumptions, far fewer domains suffice to capture banding in the 'stack of domains' model than the number of elements required in CPFEM simulations for the same purpose. This translates into much lower computational effort for the 'stack of domains' model compared to CPFEM (Arul Kumar and Mahesh, 2012).

In Arul Kumar and Mahesh (2012), the 'stack of domains' analysis was restricted to three special lattice orientations amenable to two-dimensional treatment. In the present work, this model has been modified and applied to general three-dimensional lattice orientations. The model is briefly described in Sec. 2. Lattice orientations of present interest are described and a novel method for succinct representation of their evolution during deformation is then developed in Sec. 3. The central results of the present work follow in Sec. 4: Grain subdivision and final microtexture in rolled pure copper grains, whose initial lattice orientations fall along the standard copper-type f.c.c. rolling texture fibers are predicted. Model predictions are then compared with experimental observations available in the literature in Sec. 5.

2. Model

2.1. The grain as a 'stack of domains'

The grain is represented as a one-dimensional stack of N parallelepiped shaped domains as shown schematically in Fig. 1 (Arul Kumar and Mahesh, 2012). The stacking is assumed to be repeated periodically so that domains $l = 1$ and $l = N$ are neighbors. All the domains are assumed to have the same shape and size and hence, the same volume fraction, $\rho^{[l]} = 1/N$ for $l \in \{1, 2, \ldots, N\}$. Domain boundaries are assumed to be planar and identically oriented perpendicular to the normal vector $\boldsymbol{\nu}$. In the following, indices surrounded by square brackets, e.g., $[l]$, refer to domains, while those surrounded by round brackets, e.g., (l), pertain to domain boundaries.

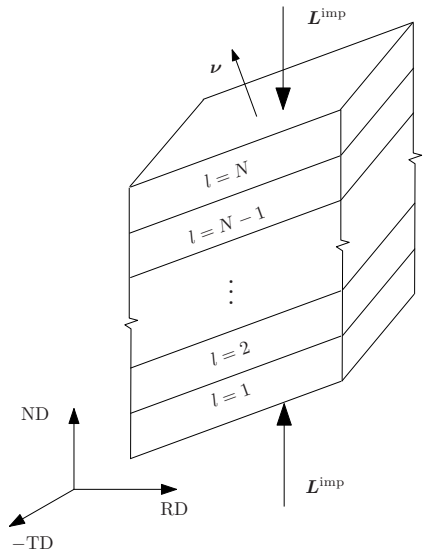

Figure 1: Representation of the model grain as a stack of N parallelepiped-shaped domains.

Each domain is assumed to deform homogeneously following standard rigid-plastic rate-independent crystal plasticity (Mahesh, 2010). A uniform lattice orientation, denoted $\boldsymbol{\Omega}^{[l]}$, is assumed in each domain l. Let $\dot{\gamma}_s^{[l]}$ and $\tau_s^{[l]}$ denote the slip-rate and critical resolved shear stress (CRSS) of slip system $s \in \{1, 2, \ldots, S\}$ in domain l, respectively. Let $\boldsymbol{b}_s^{[l]}$ and $\boldsymbol{n}_s^{[l]}$ denote the unit slip direction and unit slip plane normal. According to Schmid's law (Kocks et al., 1998),

$$\dot{\gamma}_s^{[l]} \begin{cases} \geq 0, & \text{if } \boldsymbol{\sigma}^{[l]} : \boldsymbol{b}_s^{[l]} \otimes \boldsymbol{n}_s^{[l]} = \tau_s^{[l]} \\ = 0, & \text{if } \boldsymbol{\sigma}^{[l]} : \boldsymbol{b}_s^{[l]} \otimes \boldsymbol{n}_s^{[l]} < \tau_s^{[l]}, \end{cases} \tag{1}$$

where $\boldsymbol{\sigma}^{[l]}$ denotes the uniform deviatoric stress in domain l. The slip rate tensor of domain l, $\boldsymbol{L}_{\text{ss}}^{[l]}$, is then:

$$\boldsymbol{L}_{\text{ss}}^{[l]} = \sum_{s=1}^{S} \dot{\gamma}_s^{[l]} \boldsymbol{b}_s^{[l]} \otimes \boldsymbol{n}_s^{[l]}, \tag{2}$$

and its rate of deformation, $\dot{\boldsymbol{\epsilon}}^{[l]} = (\boldsymbol{L}_{\text{ss}}^{[l]} + \boldsymbol{L}_{\text{ss}}^{[l]^T})/2$. The plastic power, P,

associated with the deformation of the 'stack of domains' is given by

$$P = \sum_{l=1}^{N} \rho^{[l]} \boldsymbol{\sigma}^{[l]} : \dot{\boldsymbol{\epsilon}}^{[l]} = \sum_{l=1}^{N} \sum_{s=1}^{S} \rho^{[l]} \tau_s^{[l]} \dot{\gamma}_s^{[l]}. \tag{3}$$

The velocity gradient of domain l, $\boldsymbol{L}^{[l]}$, is the sum of its slip-rate tensor and skew-symmetric lattice spin tensor, $\dot{\boldsymbol{W}}^{[l]}$:

$$\boldsymbol{L}^{[l]} = \boldsymbol{L}_{\mathrm{ss}}^{[l]} + \dot{\boldsymbol{W}}^{[l]}. \tag{4}$$

The two conditions to be satisfied collectively by the domains are next considered. First, the velocity gradient imposed on the model 'stack of domains' grain, $\boldsymbol{L}^{\mathrm{imp}}$, is to be accommodated collectively by all the domains:

$$\boldsymbol{L}^{\mathrm{imp}} = \sum_{l=1}^{N} \rho^{[l]} \boldsymbol{L}^{[l]}. \tag{5}$$

In the present work, plane strain compression is the imposed macroscopic deformation. It follows from the Taylor (1938) model that each grain undergoes plane strain compression, i.e.,

$$[\boldsymbol{L}^{\mathrm{imp}}]_{\mathrm{RD-TD-ND}} = \begin{bmatrix} 1 & 0 & 0 \\ 0 & 0 & 0 \\ 0 & 0 & -1 \end{bmatrix}, \tag{6}$$

where RD, TD and ND denote the rolling, transverse and normal directions associated with plane strain compression. A scalar measure of the imposed deformation is given by the von Mises strain:

$$\epsilon_{\mathrm{vM}} = \int_0^t \sqrt{\frac{2}{3} \dot{\boldsymbol{\epsilon}}^{\mathrm{imp}} : \dot{\boldsymbol{\epsilon}}^{\mathrm{imp}}}\, dt, \tag{7}$$

where,

$$[\dot{\boldsymbol{\epsilon}}^{\mathrm{imp}}]_{\mathrm{RD-TD-ND}} = [(\boldsymbol{L}^{\mathrm{imp}} + \boldsymbol{L}^{\mathrm{imp}^T})/2]_{\mathrm{RD-TD-ND}} = \begin{bmatrix} 1 & 0 & 0 \\ 0 & 0 & 0 \\ 0 & 0 & -1 \end{bmatrix}. \tag{8}$$

Second, velocity and traction continuity is demanded across domain boundaries. Velocity continuity across the domain boundary (l) between domains [l]

and $[m] = l + 1 \bmod N$ is (Hill, 1961) demands:

$$\boldsymbol{L}^{[m]} - \boldsymbol{L}^{[l]} = \boldsymbol{\lambda}^{(l)} \otimes \boldsymbol{\nu}. \tag{9}$$

where $\boldsymbol{\lambda}^{(l)}$ is the Hadamard characteristic segment of domain boundary l. Traction continuity across domain boundary (l) oriented normal to $\boldsymbol{\nu}$ requires (Arul Kumar et al., 2011):

$$\left\{(\boldsymbol{\sigma}^{[m]} - \boldsymbol{\sigma}^{[l]}) - \boldsymbol{\nu} \otimes (\boldsymbol{\sigma}^{[m]} - \boldsymbol{\sigma}^{[l]})\boldsymbol{\nu}\right\} \boldsymbol{\nu} = \boldsymbol{0}. \tag{10}$$

The lattice spin of domain l, $\dot{\boldsymbol{W}}^{[l]}$, evolves according to Eqs. (5) and Eq. (9); a closed-form expression applicable to the present 'stack of domains' model has been given in (Arul Kumar et al., 2011; Arul Kumar and Mahesh, 2012). The lattice orientation of domain l, $\boldsymbol{\Omega}^{[l]}$, evolves as

$$\dot{\boldsymbol{\Omega}}^{[l]} = \dot{\boldsymbol{W}}^{[l]} \boldsymbol{\Omega}^{[l]}. \tag{11}$$

The lattice misorientation across domain boundary (l) separating neighboring domains $[l]$ and $[m] = l + 1 \bmod N$ is (Kocks et al., 1998)

$$\omega_{(l)} = \arccos\left[(\mathrm{trace}({\boldsymbol{\Omega}^{[l]}}^T \boldsymbol{\Omega}^{[m]}) - 1)/2\right], \tag{12}$$

Differentiating this equation with respect to time, performing standard tensor algebra operations using Eq. (11), and using $\sin\omega_{(l)} = \sqrt{1 - \cos^2\omega_{(l)}}$ yields

$$\dot{\omega}_{(l)} = \frac{(\dot{\boldsymbol{W}}^{[l]} - \dot{\boldsymbol{W}}^{[m]}) : (\boldsymbol{\Omega}^{[l]} {\boldsymbol{\Omega}^{[m]}}^T)}{\sqrt{4 - (\mathrm{trace}({\boldsymbol{\Omega}^{[l]}}^T \boldsymbol{\Omega}^{[m]}) - 1)^2}}. \tag{13}$$

$\dot{\omega}_{(l)} > 0$ implies that the lattice mis-orientation between domains $[l]$ and $[m]$ across the domain boundary (l) increases. In other words, $\dot{\omega}_{(l)} > 0$ implies that the lattice orientations of domains $[l]$ and $[m]$ diverge from each other. If so, the domain boundary (l) between domains $[l]$ and $[m]$ is said to be orientationally unstable. If, however,

$$\dot{\omega}_{(l)} \leq 0, \tag{14}$$

domain boundary (l) is said to be orientationally stable. The set of domains between two nearest orientationally unstable domain boundaries are regarded as a band. Orientation gradients develop across orientationally unstable domain boundaries.

2.2. Slip system hardening

The critical resolved shear stress of the s-th slip system of domain l is taken to evolve as (Kocks et al., 1998)

$$\dot{\tau}_s^{[l]} = \frac{d\tau^{[l]}}{d\Gamma^{[l]}} \sum_{s'=1}^{S} H_{ss'}^{[l]} \dot{\gamma}_{s'}^{[l]}, \tag{15}$$

where $H_{ss'}^{[l]}$ is an element of the hardening matrix and

$$\Gamma^{[l]} = \sum_{s=1}^{S} \gamma_s^{[l]} \tag{16}$$

denotes the slip accumulated in all the slip systems of domain $[l]$. $\tau^{[l]}$ is taken to follow the Swift law (Kanjarla et al., 2010),

$$\tau^{[l]}(\Gamma^{[l]}) = \tau_0 \left(1 + \Gamma^{[l]}/\Gamma_0\right)^n, \tag{17}$$

where τ_0, Γ_0 and n are material parameters. $H_{ss'}^{[l]}$ depends on the substructure of domain l, as described below.

The hardening law given by Eq. (17) differs from the extended Voce law used in Arul Kumar and Mahesh (2012). This modification has the effect of decreasing computational time. However, as already noted in Arul Kumar and Mahesh (2012), the form of the hardening law, $\tau^{[l]}$, hardly affects banding predictions. Of much greater importance is the hardening matrix $H_{ss'}$. For several sample lattice orientations, it has been verified that banding predictions are substantially similar regardless of whether the present Swift law or the previous extended Voce law is used, if $H_{ss'}$ is the same.

2.3. Substructure in f.c.c. domains

The present model takes into account two types of sub-structure in each f.c.c. domain undergoing $\{111\}\langle 110\rangle$ slip: (i) dislocation cells or non-crystallographic dislocation walls and (ii) crystallographic dislocation walls. Following Winther and Huang (2007), it is assumed that type (ii) sub-structure forms only when slip activity is predominantly confined to a single $\{111\}$ plane. Additionally, it

is recognized that the substructure within shear bands differs from that without (Arul Kumar and Mahesh, 2012, §2.2), due to the activation of mechanisms such as dynamic recovery (Korbel and Szczerba, 1982) and deformation twinning (Huang et al., 2006) within shear bands, even at quasistatic strain-rates in coarse grained material. The sub-structure within shear bands is therefore, classified separately as type (iii).

The effective slip accumulated in each of the four $\{111\}$ planes is defined as the sum of the slips in the $\langle 110 \rangle$ slip systems associated with it, excluding those slip systems whose cross-slip systems are also activated (Mahesh, 2006; Arul Kumar and Mahesh, 2012). The latter slip systems are excluded because screw dislocations gliding in one of a pair of simultaneously activated cross-slip systems may cross-slip onto the other and are, therefore, unlikely to be trapped in their original glide plane. Let $\Delta\Gamma^{[l]}_{p^*}$ and $\Delta\Gamma^{[l]}_{p^{**}}$ denote the largest and second largest effective slips, respectively, amongst those accumulated in the four $\{111\}$ planes of domain $[l]$ over a prescribed imposed von Mises strain increment $\Delta\epsilon_{\mathrm{vM}}$. The slip plane p^* is said to be dominant if

$$\Delta\Gamma^{[l]}_{p^*}/\Delta\Gamma^{[l]}_{p^{**}} \geq R, \tag{18}$$

where R is a prescribed constant. The condition for slip plane dominance, Eq. (18), deviates from the condition given by Arul Kumar and Mahesh (2012), which was in terms of a ratio of total accumulated slip. The present condition is better in that it accounts for changes in slip activity during deformation caused e.g., by lattice rotations or load-path changes.

If Eq. (18) is not satisfied, it is assumed following Winther and Huang (2007) that the domain sub-structure is of type (i), which is assumed to produce negligible plastic anisotropy:

$$H^{(\mathrm{i})}_{ss'} = 1, \quad s, s' \in \{1, 2, \ldots, S\} \tag{19}$$

On the other hand, if Eq. (18) is satisfied, a type (ii) substructure with crystallographic dislocation walls is assumed to form parallel to p^*. The plastic anisotropy produced by these barriers is accounted for by setting the hardening

matrix, $[H^{(\mathrm{ii})}]$, as

$$H^{(\mathrm{ii})}_{ss'} = \begin{cases} h \geq 1, & \text{if } \boldsymbol{n}_s \neq \pm\boldsymbol{n}_{p^*},\ \boldsymbol{n}_{s'} = \pm\boldsymbol{n}_{p^*}, s \neq s', \\ 1, & \text{otherwise.} \end{cases} \tag{20}$$

It is experimentally known that shear bands in copper can only develop in grains with a pre-existing type (ii) substructure (Nakayama and Morii, 1982). The type (iii) substructure within shear bands may reasonably be assumed to be comprised of partly recovered crystallographic dislocation walls. Accordingly, the type (iii) hardening matrix is taken to be

$$H^{(\mathrm{iii})}_{ss'} = \chi H^{(\mathrm{ii})}_{ss'}, \quad s, s' \in \{1, 2, \ldots, S\}, \tag{21}$$

where, $0 \leq \chi \leq 1$ indicates a reduced hardening rate in domains representing shear bands due to recovery effects. It is emphasized that Eq. (21) implies only reduced hardening of the slip systems in the shear band, not softening.

2.4. Identification of bands

As noted above, a type (ii) substructure is experimentally known to be a necessary pre-condition for the formation of a shear band (Nakayama and Morii, 1982). If all the domains of the model grain have a type (ii) substructure with the same dominant slip plane p^*, any bands predicted following Eq. (14) are identified as shear bands. Otherwise, the predicted bands are identified as deformation bands.

2.5. Band boundary orientation

In Arul Kumar and Mahesh (2012), the orientation $\boldsymbol{\nu}$ of the domain boundary normal was determined using the criterion that it results in the minimization of the plastic power P, Eq. (3). Following a similar procedure in the present work is highly computationally intensive, as the space of possible $\boldsymbol{\nu}$ in the present work is one more than that in Arul Kumar and Mahesh (2012). In the present work, for imposed plane strain compression Eqs. (6) and (8), the plastic power P is calculated for each $\boldsymbol{\nu}^* \in \mathscr{N}$, where

$$\mathscr{N} = \{(\mathrm{RD} + \mathrm{ND})/\sqrt{2},\ (\mathrm{RD} - \mathrm{ND})/\sqrt{2},\ \mathrm{RD},\ \mathrm{ND}\}. \tag{22}$$

The $\boldsymbol{\nu}^*$ that minimizes P is taken to be the model domain boundary normal, $\boldsymbol{\nu}$. This methodology, which considerably reduces the computational effort of calculating $\boldsymbol{\nu}$, is justified below.

In a shear banding grain, much of the deformation is known to be confined to shear bands; plastic deformation of the matrix is relatively negligible (Wagner et al., 1995). If the number of domains representing shear bands in the model is n_{SB}, if all such domains are assumed to deform identically, and if domains representing the matrix are assumed rigid, the rate of deformation of domain $[l]$ representing a shear band would be $\dot{\boldsymbol{\epsilon}}^{[l]} = (N/n_{\mathrm{SB}})\dot{\boldsymbol{\epsilon}}^{\mathrm{imp}}$ in order to satisfy Eq. (5). The jump in the rate of displacement across the boundary between domain $[l]$, which represents a shear band and its neighboring domain $[m]$, which represents a part of the matrix would be $\dot{\boldsymbol{\epsilon}}^{[l]} - \dot{\boldsymbol{\epsilon}}^{[m]} = (N/n_{\mathrm{SB}})\dot{\boldsymbol{\epsilon}}^{\mathrm{imp}} - \mathbf{0} = (N/n_{\mathrm{SB}})\dot{\boldsymbol{\epsilon}}^{\mathrm{imp}}$. Now, the domain boundary (l) separating domains $[l]$ and $[m]$ must be so oriented that the plastic deformation of the neighboring domains is compatible. Mahesh (2012) has shown that this is achieved for $\boldsymbol{\nu} = (\boldsymbol{v}_1 \pm \boldsymbol{v}_2)/\sqrt{2}$, where $\boldsymbol{v}_1$ and $\boldsymbol{v}_2$ are the unit eigenvectors corresponding to the largest and smallest eigenvalues, respectively, of $\dot{\boldsymbol{\epsilon}}^{[l]} - \dot{\boldsymbol{\epsilon}}^{[m]} = (N/n_{\mathrm{SB}})\dot{\boldsymbol{\epsilon}}^{\mathrm{imp}}$. This yields $\boldsymbol{\nu} = (\mathrm{RD} \pm \mathrm{ND})/\sqrt{2}$ for $\dot{\boldsymbol{\epsilon}}^{\mathrm{imp}}$ given by Eq. (8).

This conclusion about the orientation of shear band boundaries accords well with experimental observations. In shear banded single crystals subjected to plane strain deformation, band boundaries have been experimentally observed to align approximately along $\boldsymbol{\nu} = (\mathrm{RD} \pm \mathrm{ND})/\sqrt{2}$ (Nakayama and Morii, 1982; Wagner et al., 1995; Jasienski et al., 1996).

In a deformation banding grain under plane strain compression, Lee and Duggan (1993); Lee et al. (1993) and Wert and Huang (2003) have suggested that the rate of deformation of neighboring bands differs by a redundant shear in the RD–ND plane, i.e.,

$$[\dot{\boldsymbol{\epsilon}}^{[l]} - \dot{\boldsymbol{\epsilon}}^{[m]}]_{\mathrm{RD-TD-ND}} = \begin{bmatrix} 0 & 0 & X \\ 0 & 0 & 0 \\ X & 0 & 0 \end{bmatrix}, \tag{23}$$

for non-zero X. Applying the criterion of Mahesh (2012), it can be seen that compatibility requires either $\boldsymbol{\nu} = \mathrm{RD}$ or $\boldsymbol{\nu} = \mathrm{ND}$. This conclusion accords with experimental observations: in deformation banded grains, band boundaries have been observed to align with the rolling plane, $\boldsymbol{\nu} = \mathrm{ND}$ (Heye and Sattler, 1971; Liu and Hansen, 1998).

3. Lattice orientations

3.1. Texture fibers

Table 1: Texture fibers under study. Values of a_1, b_1, c_1, a, b and c are given in the text.

Fiber $\mathscr{F}$	Free parameter $\xi \in [\xi^0, \xi^1]$	Fixed parameters
α	$\Phi_1 \in [0°, 90°]$	$\Phi = 45°$, $\Phi_2 = 0°$
β	$\Phi_2 \in [45°, 90°]$	$\Phi_1 = a_1\Phi_2^2 - b_1\Phi_2 + c_1$ $\Phi = a\Phi_2^2 - b\Phi_2 + c$
τ	$\Phi \in [0°, 90°]$	$\Phi_1 = 90°$, $\Phi_2 = 45°$

Simulations of plane strain deformation are performed on grains whose lattice orientations are drawn from the standard copper type f.c.c. rolling texture fibers (Engler and Randle, 2010). A texture fiber is a collection of lattice orientations, which describe a continuous curve in the space of lattice orientations: $\mathscr{F} = \{\boldsymbol{\Omega}_\xi : \xi \in [\xi^0, \xi^1]\}$. $\boldsymbol{\Omega}_\xi$ may be specified by Euler angles (Φ_1, Φ, Φ_2). The Euler angles that describe the three standard texture fibers of present interest are listed in Tab. 1, following Bunge convention (Engler and Randle, 2010). The curve of maximum intensity, which defines the β fiber (Hirsch and Lucke, 1988), is well-approximated by a quadratic polynomial. Its coefficients, $a_1 = 1.76 \times 10^{-2}/°$, $b_1 = 0.4876$, $c_1 = 46.645°$, $a = 5.2 \times 10^{-3}/°$, $b = 3.5861$ and $c = 215.83°$, are obtained by least-squares fitting.

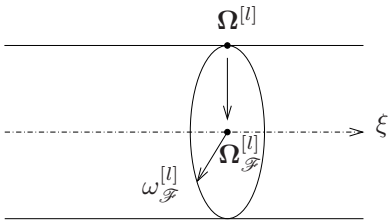

Figure 2: Schematic diagram of lattice orientation space showing the dash-dot line indicating fiber $\mathscr{F}$, domain lattice orientation, $\mathbf{\Omega}^{[l]}$, and its projection onto the fiber, $\mathbf{\Omega}^{[l]}_{\mathscr{F}}$.

3.2. Projection of lattice orientations onto fibers

The misorientation between the lattice orientation of domain l, $\mathbf{\Omega}^{[l]}$ and another lattice orientation $\mathbf{\Omega} \in SO(3)$ is given by the formula (Kocks et al., 1998)

$$\theta(\mathbf{\Omega}, \mathbf{\Omega}^{[l]}) = \arccos\left[(\mathrm{trace}(\mathbf{\Omega}^T \mathbf{\Omega}^{[l]}) - 1)/2\right], \tag{24}$$

where $0 \leq \theta(\mathbf{\Omega}, \mathbf{\Omega}^{[l]}) \leq 180^\circ$ without loss of generality. The projection of $\mathbf{\Omega}^{[l]}$ onto fiber $\mathscr{F}$ is defined as a fiber orientation, $\mathbf{\Omega}^{[l]}_{\mathscr{F}}$, that is minimally misoriented with respect to $\mathbf{\Omega}^{[l]}$, as shown in Fig. 2:

$$\mathbf{\Omega}^{[l]}_{\mathscr{F}} = \underset{\mathbf{\Omega} \in \mathscr{F}}{\mathrm{argmin}} \ \theta(\mathbf{\Omega}, \mathbf{\Omega}^{[l]}). \tag{25}$$

Also, the misorientation between $\mathbf{\Omega}^{[l]}$ and its projection, $\mathbf{\Omega}^{[l]}_{\mathscr{F}}$, is

$$\omega^{[l]}_{\mathscr{F}} = \theta(\mathbf{\Omega}^{[l]}_{\mathscr{F}}, \mathbf{\Omega}^{[l]}) = \min_{\mathbf{\Omega} \in \mathscr{F}} \theta(\mathbf{\Omega}, \mathbf{\Omega}^{[l]}). \tag{26}$$

Parameter ξ corresponding to $\mathbf{\Omega}^{[l]}_{\mathscr{F}}$ in the fiber is denoted $\xi^{[l]}_{\mathscr{F}}$. The scalars $\xi^{[l]}_{\mathscr{F}}$ and $\omega^{[l]}_{\mathscr{F}}$ locate $\mathbf{\Omega}^{[l]}$ in relation to $\mathscr{F}$, on a circle of radius $\omega^{[l]}_{\mathscr{F}}$ centered at $\xi^{[l]}_{\mathscr{F}}$, as shown schematically in Fig. 2. Variation of $\xi^{[l]}_{\mathscr{F}}$ and $\omega^{[l]}_{\mathscr{F}}$ with deformation provides a concise description of the lattice rotation of domain l along the fiber and out of the fiber, respectively. This description will be used in Sec. 4.

3.3. Euclidean average lattice orientation

The Euclidean average of a set of lattice orientations $\{\mathbf{\Omega}^{[l]}, l = 1, 2, \ldots, N\}$ is defined as (Moakher, 2002)

$$\mathbf{\Omega}^{\mathrm{E}} = \underset{\mathbf{\Omega}\in SO(3)}{\operatorname{argmin}} \sum_{l=1}^{N} \|\mathbf{\Omega}^{[l]} - \mathbf{\Omega}\|_F, \tag{27}$$

where, $\|\cdot\|_F$ denotes the Frobenius norm. Moakher (2002) has also provided an elegant algorithm for the computation of $\mathbf{\Omega}^{\mathrm{E}}$. The projection of $\mathbf{\Omega}^{\mathrm{E}}$ onto fiber $\mathscr{F}$ is denoted $\mathbf{\Omega}^{\mathrm{E}}_{\mathscr{F}} = \underset{\mathbf{\Omega}\in\mathscr{F}}{\operatorname{argmin}} \ \theta(\mathbf{\Omega}, \mathbf{\Omega}^{\mathrm{E}})$. The scalar parameter that identifies $\mathbf{\Omega}^{\mathrm{E}}_{\mathscr{F}}$ on the fiber is denoted $\xi^{\mathrm{E}}_{\mathscr{F}}$. Further, paralleling Eq. (26), $\omega^{\mathrm{E}}_{\mathscr{F}} = \theta(\mathbf{\Omega}^{\mathrm{E}}_{\mathscr{F}}, \mathbf{\Omega}^{\mathrm{E}})$ is also defined.

3.4. Scalar measures of banding

Groups of neighboring domains in a model grain that are bounded by orientationally unstable domain boundaries have been recognized as shear bands or deformation bands in the present model, as described in Sec. 2.4. This classification methodology, however, differs from that used for the experimental identification of these bands from micrographs. Experimentally, deformation bands are recognized by observing a repetitive pattern of highly misoriented regions in micrographs (Lee and Duggan, 1993; Kulkarni et al., 1998). Likewise, shear bands are recognized in micrographs as narrow regions that have high shear relative to the matrix (Wagner et al., 1995). Anticipating the comparison with experimental data in the next section, two scalar measures of banding in a grain are now introduced, on the basis of which, shear banding and deformation banding of model grains can be identified as in the experimental approach.

The average deviation of domain lattice orientations from $\mathbf{\Omega}^{\mathrm{E}}$ is defined as

$$\bar{\mu} = \sum_{l=1}^{N} \theta(\mathbf{\Omega}^{[l]}, \mathbf{\Omega}^{\mathrm{E}})/N. \tag{28}$$

A large value of $\bar{\mu}$ indicates that the typical domain in the model grain deviates substantially from the average lattice orientation of the model grain. This will be taken to indicate deformation banding. A small value of $\bar{\mu}$ is inconclusive by

itself; it may indicate either shear banding or homogeneous grain deformation. Since deformation band boundaries are observed to be large angle dislocation boundaries in experimental observations (Heye and Sattler, 1971; Bauer et al., 1977; Wróbel et al., 1988, 1993, 1994; Liu and Hansen, 1998; Liu et al., 2000; Wert, 2002), model grains for which $\bar{\mu} \geq 10^\circ$ are taken to be deformation banded presently.

Likewise, a parameter to identify shear localization based on instantaneous observation of the model grain, as in experiments is introduced. Localization of slip in a few domains is quantified using the parameter

$$L = \max_{l=1,2,\ldots N} \Gamma^{[l]} / \underset{l=1,2,\ldots N}{\text{median}} \ \Gamma^{[l]} \geq 1. \tag{29}$$

In a shear banding grain, it is expected that $\max_{l=1,2,\ldots N} \Gamma^{[l]}$ is realized in the domain representing the shear band and $\underset{l=1,2,\ldots N}{\text{median}} \ \Gamma^{[l]}$ is realized in a typical domain of the matrix. A large value of L indicates substantial slip localization, i.e., shear banding, while a small value of L indicates a lack thereof.

The critical value of L for shear banding is obtained using an approximate calculation based on data reported by Wagner et al. (1995, Sec. 3.2, 5.1) in Al 1.8%Cu; they found that microshear bands of typical thickness $d = 2.5$ μm separated by a typical distance of $l = 125$ μm undergo shear of ~ 3 over a macroscopic strain increment of about 0.02. This gives a value of $\sim 3d/l = 0.06$ for the shear band strain. The value of L in the shear banding crystal of Wagner et al. (1995) is therefore estimated as $0.06/0.02 = 3$. Accordingly, in the sequel, grains for which $L \geq 3$ will be taken to shear band.

4. Results

Each of the fibers described above is discretized in steps $\Delta\xi = 1^\circ$ to obtain nominal initial lattice orientations of the presently studied grains. Each model grain is discretized into $N = 22$ domains. For certain representative lattice orientations, it has been verified that the predictions assuming discretization into 22 domains agrees closely with that assuming finer discretization into 44 domains.

It is necessary to supply an initial numerical perturbation to the domains in order that inhomogeneity may develop during the simulated deformation. Accordingly, the initial lattice orientation of each domain is perturbed from the nominal grain lattice orientation by 0.5° about a rotation axis chosen randomly from a uniform distribution over the unit sphere.

Table 2: Parameter values.

Parameter	Reference	Value
τ_0	Eq. (17), Kanjarla et al. (2010)	16 MPa
Γ_0	Eq. (17), Kanjarla et al. (2010)	0.0275
n	Eq. (17), Kanjarla et al. (2010)	0.5
$\Delta\epsilon_{\mathrm{vM}}$	Sec. 2.3	0.05
R	Eq. (18)	130
h	Eq. (20)	3.1
χ	Eq. (21)	0.4

Deformation of grains by plane strain compression following Eq. (6) to $\epsilon_{\mathrm{vM}} = 0.5$ is simulated. Values of the various model parameters for pure copper are given in Tab. 2.

4.1. Banding

The variation of the two scalar measures of banding, $\bar{\mu}$ and L, defined in Sec. 3.4 along the three texture fibers is shown in Fig. 3. The horizontal axis in these figures indicates $\xi(0)$, the nominal initial lattice orientations along the fibers. Standard named lattice orientations – G (Goss), B (Brass), A, P, RG (rotated Goss), C (copper), S, NRC (normal rotated cube) and D (Dillamore) – are marked in the upper horizontal axis.

Taking $\bar{\mu} \geq 10°$ to indicate deformation banding and $L \geq 3$ to indicate shear banding for reasons given in Sec. 3.4, the three texture fibers are subdivided into distinct homogeneously deforming (H), deformation banding (DB) and shear banding (SB) segments in Fig. 3. Shear banding is not predicted in the α fiber

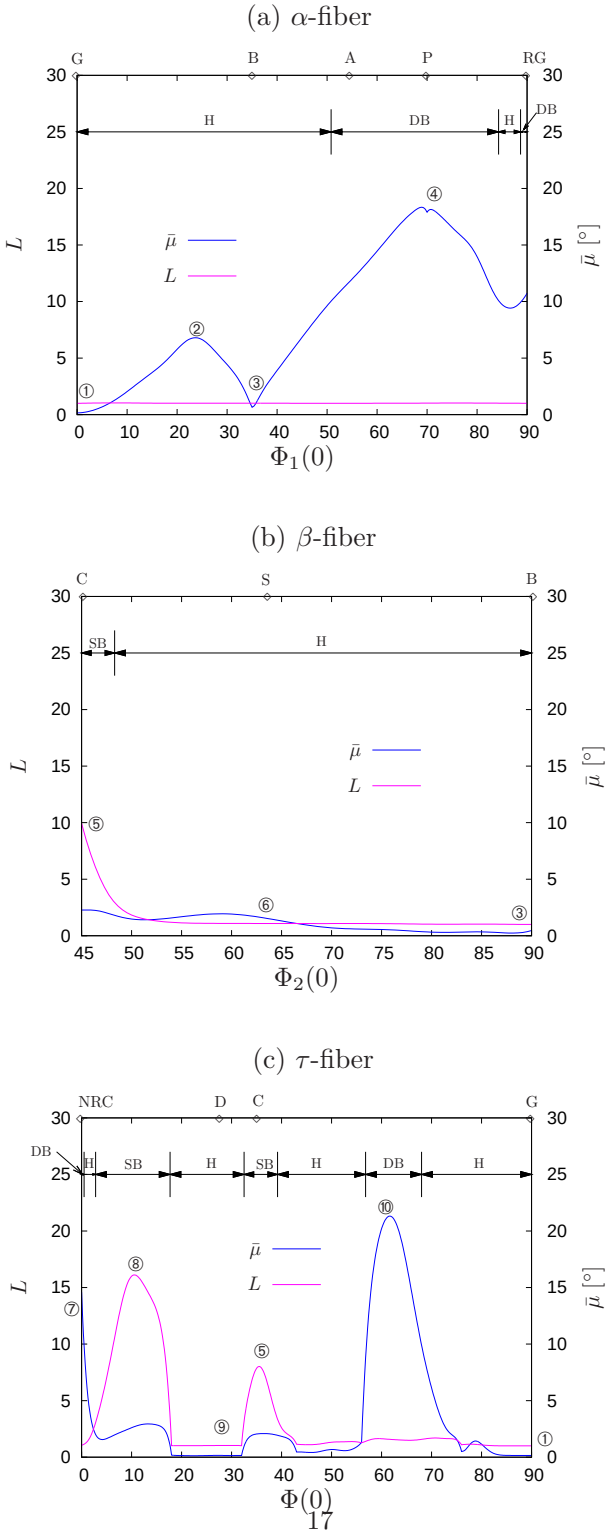

Figure 3: Variation of $\bar{\mu}$ (Eq. (28)) and L (Eq. (29)) along the (a) α, (b) β and (c) τ fibers. Pole figures of lattice orientations labeled with numbers are shown in Fig. 4. Standard named orientations are marked on the upper horizontal axis.

and deformation banding in not predicted in the β fiber. A rich variation of banding response is predicted in the τ fiber.

4.2. Microtexture

The microtexture after plane strain deformation to $\epsilon_{\text{vM}} = 0.5$ of selected orientations marked in Fig. 3 and tabulated in Tab. 3 is now studied in detail. Initial orientations and the Taylor factor (Hosford, 1966) calculated as

$$M = \frac{\sum_{s=1}^{S} \dot{\gamma}_s}{\dot{\epsilon}^{\text{imp}}_{\text{RD}-\text{RD}}}, \tag{30}$$

for the selected orientations are listed in Tab. 3. In Eq. (30), $\dot{\gamma}_s$ denotes the slip-rate in the s-th slip system obtained by solving the Taylor model of the grain with $N = 1$ domain.

Table 3: The initial crystal orientations in Bunge angle and Miller indices notation and the Taylor factor of grains whose post-deformation {111} pole figures are shown in Fig. 4.

Grain	Initial Euler angles $(\Phi_1(0), \Phi(0), \Phi_2(0))$	(ND)/[RD]	Taylor factor M
① : G	$(0.0°, 45.0°, 0.0°)$	(011)[100]	2.45
②	$(23.0°, 45.0°, 0.0°)$	(011)[10 $\bar{3}$ 3]	3.97
③: B	$(35.2°, 45.0°, 0.0°)$	(011)[2$\bar{1}$1]	3.26
④: P	$(70.5°, 45.0°, 0.0°)$	(011)[1$\bar{2}$2]	5.24
⑤: C	$(90.0°, 35.2°, 45.0°)$	(112)[$\bar{1}\bar{1}$1]	3.67
⑥: S	$(59.0°, 36.7°, 63.4°)$	(213)[$\bar{3}\bar{6}$4]	3.49
⑦: NRC	$(90.0°, 0.0°, 45.0°)$	(001)[$\bar{1}\bar{1}$0]	2.45
⑧	$(90.0°, 10.0°, 45.0°)$	(118)[$\bar{4}\bar{4}$1]	2.34
⑨: D	$(90.0°, 27.2°, 45.0°)$	(4 4 11)[$\bar{1}$1 $\bar{1}$1 8]	3.53
⑩	$(90.0°, 60.0°, 45.0°)$	(554)[$\bar{2}\bar{2}$5]	3.61

The microtexture before and after plane strain deformation to $\epsilon_{\text{vM}} = 0.5$ of the selected orientations are shown in Fig. 4 using the standard {111} equal-area

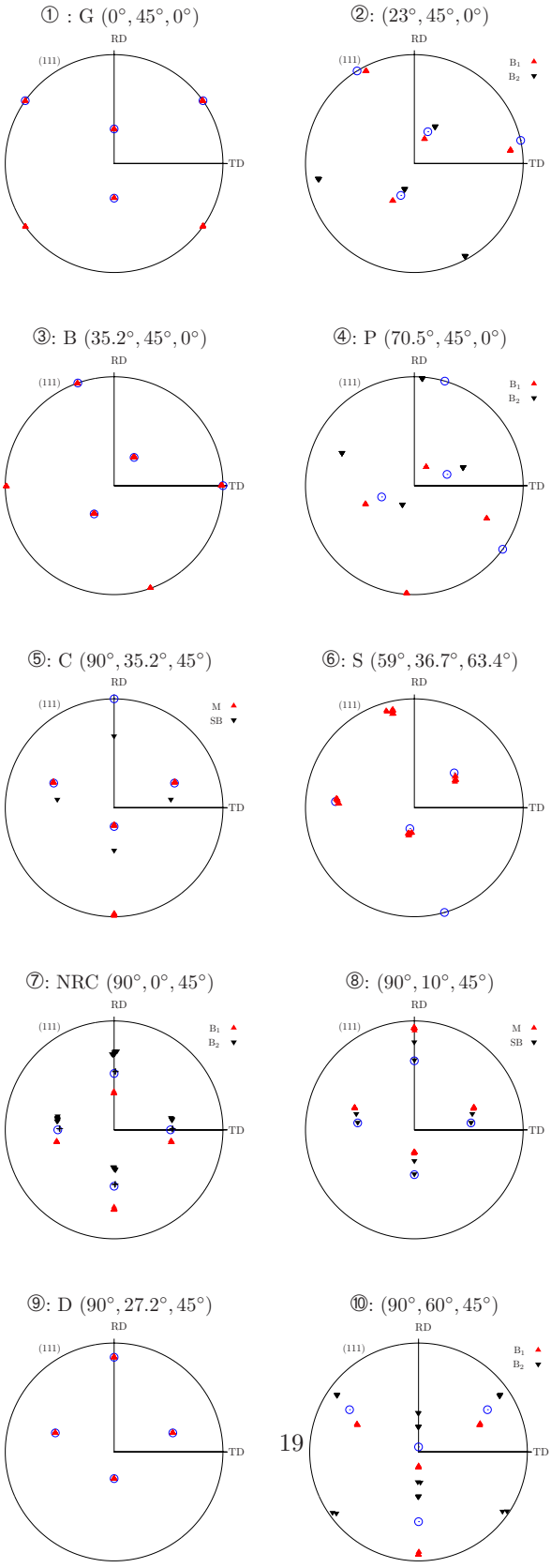

Figure 4: Pole figure representation of domain lattice orientations of model grains at $\epsilon_{\mathrm{vM}} = 0.0$ ($\odot$) and $\epsilon_{\mathrm{vM}} = 0.5$ (+, ▲, ▽). The location of all grains in the fibers are marked in Fig. 3.

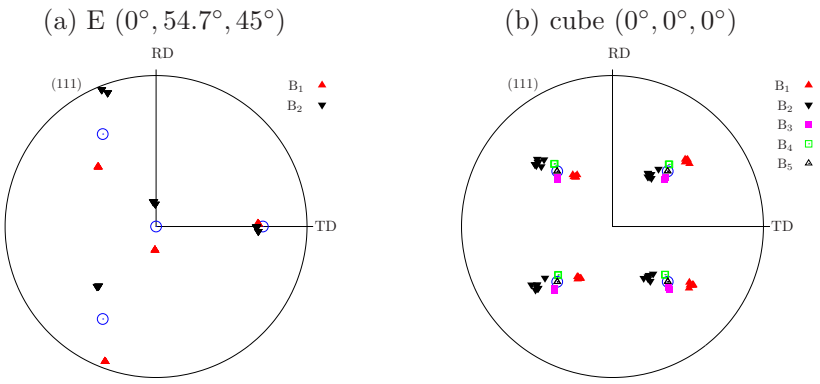

Figure 5: Pole figure representation of domain lattice orientations of model grains at $\epsilon_{\mathrm{vM}} = 0.0$ ($\odot$) and $\epsilon_{\mathrm{vM}} = 0.5$ for (a) E and (b) cube oriented copper grains. These orientations do not fall on any of the texture fibers considered.

pole figure representation. Each pole figure shows 92 poles: four {111} poles corresponding to the nominal initial orientation and four {111} poles for each of the $N = 22$ domains after deformation. The number of distinctly visible poles is, however, much smaller on account of overlap amongst the predicted poles. The microtexture before and after plane strain deformation to $\epsilon_{\mathrm{vM}} = 0.5$ of two grain orientations, E ((ND)/[RD] $= (111)[1\bar{1}0]$, Euler angles $= (0°, 54.7°, 45°)$ and Taylor factor $M = 4.08$) and cube ((ND)/[RD] $= (001)[100]$, Euler angles $= (0°, 0°, 0°)$ and Taylor factor $M = 2.45$), which do not fall in any of the three texture fibers under present consideration are also shown in Fig. 5.

Fig. 4 shows that the lattice orientation in the domains of the ① B, ③ G and ⑨ D orientations do not rotate during deformation. Such orientations are said to be stable (Kocks et al., 1998). The domain lattice orientations of the initially ② and ⑥ S oriented grains develop only a small spread with deformation, which results in their classification as homogeneously deforming grains in Sec. 4.1. Other orientations in Fig. 4 and both orientations in Fig. 5

develop a pronounced spread of lattice orientations in the course of deformation, which implied banding.

The pole figure representation of Fig. 4 provides insight into domain rotations in selected orientations along the texture fibers. It is, however, not conducive to a concise representation of the variation of the microtexture all along the fibers. An alternate representation of the microtexture after deformation is therefore given in Fig. 6, where the lattice orientations of all domains l in all model grains are shown.

Let $\xi_{\mathscr{F}}^{[l]}$ and $\omega_{\mathscr{F}}^{[l]}$ (Sec. 3.2) denote lattice orientation parameters after deformation to $\epsilon_{\mathrm{vM}} = 0.5$. Let $\xi(0)$ denote the nominal initial lattice orientation. Figs. 6 (a_1)–(a_3) and Figs. 6 (b_1)–(b_3) show $\xi_{\mathscr{F}}^{[l]}$ and $\omega_{\mathscr{F}}^{[l]}$ variation with $\xi(0)$, respectively. Besides conciseness, this representation allows (i) a simpler description of lattice rotations in the fiber-fixed $(\xi_{\mathscr{F}}^{[l]}, \omega_{\mathscr{F}}^{[l]})$ coordinate system than in the sample RD-TD-ND system and (ii) easy identification of fiber segments with similar banding behavior.

4.2.1. α fiber

In the α fiber, $\mathscr{F} = \alpha$ and $\xi_{\mathscr{F}}^{[l]} = {\Phi_1}_{\alpha}^{[l]}$ (Tab. 1). Stable lattice orientations must satisfy ${\Phi_1}_{\alpha}^{[l]} \approx \Phi_1(0)$ and $\omega_{\alpha}^{[l]} \approx 0$, $\forall l \in \{1, 2, \ldots, N\}$ and should thus plot on the 45° line in Fig. 6 (a_1) and on the horizontal axis in Fig. 6 (b_1). As these conditions are satisfied by the G and B orientations, they are classified as stable. Also, all lattice orientations in the α-fiber, except G, have a component of lattice rotation toward B, as seen in Fig. 6 (a_1). Lattice orientations, except those in the vicinity of G and B, undergo significant out of fiber lattice rotations. This lattice rotation can be as large as $\omega_{\alpha}^{[l]} = 20°$ near P (Fig. 6 (b_1)).

Figs. 6 (a) and (b) also show the ${\Phi_1}_{\alpha}^{\mathrm{E}}$ corresponding to the projection of the Euclidean average lattice orientation onto the α fiber, after deformation and its deviation $\omega_{\alpha}^{\mathrm{E}}$ from the α fiber, respectively. Except in the vicinity of the deformation banding RG orientation, ${\Phi_1}_{\alpha}^{\mathrm{E}} \approx {\Phi_1}_{\alpha}^{[l]}$, $\forall l \in \{1, 2, \ldots, N\}$, which suggests that the in fiber rotations of all domains are comparable. However, $\omega_{\alpha}^{\mathrm{E}} \approx 0$ (Fig. 6 (b)). Thus, even though the lattice orientations of individual domains

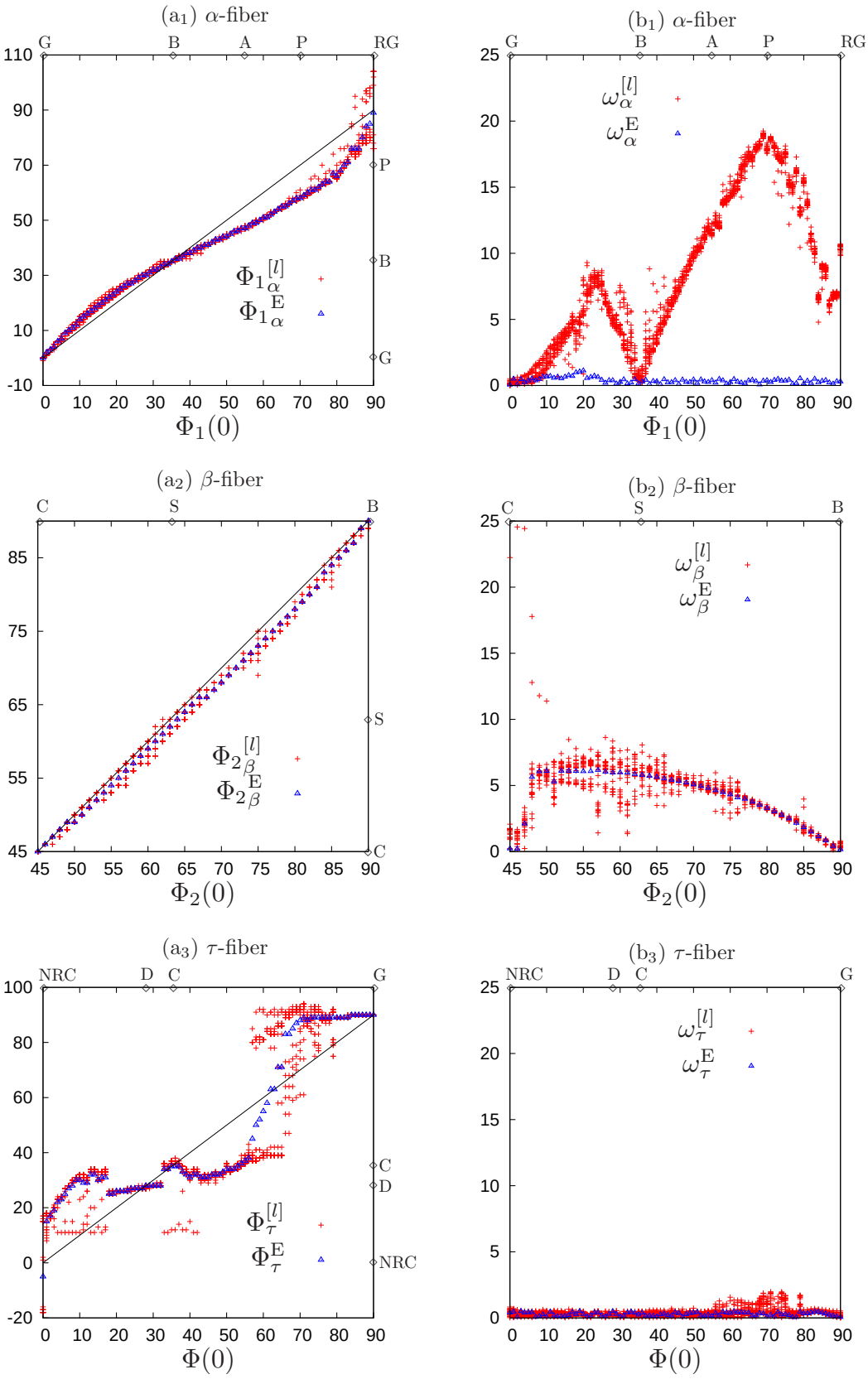

Figure 6: Representation of the deformed microtexture of grains initially oriented along the (a_1), (b_1) α, (a_2), (b_2) β and (a_3), (b_3) τ fibers. (a_1), (a_2) and (a_3) show rotations along the fibers, while (b_1), (b_2) and (b_3) show rotations out of the fibers. The unit on all axes is °. Both abscissa and ordinate of each plotted point is rounded to the nearest degree.

may deviate substantially from the α fiber, the Euclidean average lattice orientation remains on the fiber. This indicates that domain lattice rotations are symmetrical about the fiber.

4.2.2. β fiber

In the β fiber, $\mathscr{F} = \beta$ and $\xi_{\mathscr{F}}^{[l]} = {\Phi_2}_{\beta}^{[l]}$ (Tab. 1). B is the only stable orientation in the β fiber. Other orientations undergo lattice rotations both along and out of the fiber, as indicated by ${\Phi_2}_{\beta}^{[l]} \neq \Phi_2(0)$ in Fig. 6 (a_2) and $\omega_{\beta}^{[l]} > 0$ in Fig. 6 (b_2). The out of fiber rotations are larger than the in fiber rotations.

In grains near the shear banding C orientation a few domains (one or two) undergo large out of fiber rotations, as indicated by $\omega_{\beta}^{[l]} > 10^\circ$ in Fig. 6(a_2). Other domains in these grains undergo much smaller out of fiber rotations. Slip localizes in domains undergoing significant rotations so that these domains do indeed comprise the shear bands.

In the range $50^\circ < \Phi_2 \leq 90^\circ$, the maximum out of fiber domain rotation, $\max_l \omega_{\beta}^{[l]} < 10^\circ$. This deviation diminishes and vanishes in the range $70^\circ < \Phi_2 \leq 90^\circ$ as the stable B orientation is approached. This accords with the observation in Sec. 4.1 that in the range $50^\circ < \Phi_2 \leq 90^\circ$, grains undergo neither shear banding nor significant deformation banding.

4.2.3. τ fiber

In the τ fiber, $\mathscr{F} = \tau$ and $\xi_{\mathscr{F}}^{[l]} = \Phi_{\tau}^{[l]}$ (Tab. 1). D ($\Phi = 27.2^\circ$) and G ($\Phi = 90^\circ$) are the only stable orientations in the τ fiber because they satisfy $\Phi_{\tau}^{[l]} \approx \Phi(0)$ and $\omega_{\tau}^{[l]} \approx 0$, $\forall l \in \{1, 2, \ldots, N\}$ (Figs. 6 (a_3) and (b_3)).

Lattice orientations other than D and G undergo rotation during deformation. Unlike in the foregoing α and β fibers, domain lattice rotations in the τ fiber are predominantly along the fiber. Out of fiber rotations are negligible, as indicated by $\omega_{\tau}^{[l]} \approx 0$, $\forall l \in \{1, 2, \ldots, N\}$ in Fig. 6 (b_3).

Fig. 6 (a_3) shows that grains in the vicinity of D ($20^\circ \leq \Phi \leq 32^\circ$) rotate toward D ($\Phi = 27.2^\circ$) and grains in the vicinity of G ($80^\circ \leq \Phi \leq 90^\circ$) rotate

toward G. Also, grains with $43^\circ \leq \Phi \leq 56^\circ$ rotate toward the C orientation ($\Phi = 35.2^\circ$). Moreover, $\Phi_\tau^{[l]} = \Phi_\tau^{\mathrm{E}}$ and $\omega_\tau^{[l]} = \omega_\tau^{\mathrm{E}} = 0$ for these lattice orientations. It follows that these grains deform homogeneously.

Domains of the NRC orientation ($\Phi = 0^\circ$) undergo large rotations in opposite directions along the τ fiber (Fig. 6 (a_3)). This behavior, however, persists only over $0^\circ \leq \Phi \leq 1^\circ$.

In the range $57^\circ \leq \Phi \leq 70^\circ$, approximately half the domains of the grain rotate toward C ($\Phi = 35.2^\circ$) and the other half rotate toward G ($\Phi = 90^\circ$) along the τ-fiber (Fig. 6 (a_3)). This produces pronounced deformation banding (Sec. 4.1).

In $71^\circ \leq \Phi \leq 79^\circ$ the lattice rotation of the domains is qualitatively similar to that of the deformation banding grains in $57^\circ \leq \Phi \leq 70^\circ$, except that lattice rotations toward G are more pronounced than those toward C. In this range of lattice orientations a smooth transition from pronounced deformation banding of the preceding range $57^\circ \leq \Phi \leq 70^\circ$ to homogeneous deformation of the succeeding range $80^\circ \leq \Phi \leq 90^\circ$ appears to be underway.

Finally, in $3^\circ \leq \Phi \leq 17^\circ$ and $33^\circ \leq \Phi \leq 40^\circ$, a few domains (one or two) rotate significantly away from the remaining domains (Fig. 6 (a_3)). These domains undergo intense slip localization and constitute the model shear band, noted in Sec. 4.1.

5. Discussion

The 'stack of domains' model of a grain has been been employed to study the banding response and microtexture development in pure copper subjected to rolling deformation to von Mises strain $\epsilon_{\mathrm{vM}} = 0.5$. Lattice orientations along the α, β and τ fibers have been analyzed. The present model does not address or model the dislocation rearrangement necessary to form deformation or shear bands; it assumes that the necessary rearrangement of the dislocation sub-structure will occur if the energetics of grain deformation makes banding more favorable than homogeneous deformation.

5.1. Comparison with experimental observations in single crystals

The predicted banding response of the G, B, NRC, C and S oriented grains that fall in one of the three fibers are now compared with experimental observations for pure copper in the literature. This comparison is also carried out for the E and cube orientations, which do not fall on the fibers considered above.

5.1.1. Homogeneous deformation

G (Bauer et al., 1977; Malin et al., 1981; Nakayama and Morii, 1982; Wróbel et al., 1993, 1994, 1996) and B (Jago and Hatherly, 1975; Grewen et al., 1977; Bauer et al., 1977; Malin et al., 1981; Nakayama and Morii, 1982; Wróbel et al., 1993, 1994) oriented copper single crystals are experimentally observed to deform homogeneously and to remain stable with deformation. The present 'stack of domains' model also predicts homogeneous deformation as indicated by $\bar{\mu} = 0.15°$ and $L = 1.001$ for G and $\bar{\mu} = 0.65°$ and $L = 1.007$ for B.

In an initially coarse grained copper polycrystal rolled 85%, Lee and Duggan (1993) report frequent observations of the S orientation. This suggests that S oriented grains do not deformation band. In accord with this observation, the present calculations predict no deformation banding in the S grains, as indicated by $\bar{\mu} = 3°$.

5.1.2. Deformation banding

NRC copper single crystals are known experimentally to deformation band during plane strain compression (Heye and Sattler, 1971; Bauer et al., 1977; Wróbel et al., 1988, 1993, 1994). This is also predicted presently by the high value of $\bar{\mu} = 14.6°$ and the low value of $L = 1.03$. Deformation banding initiates in this grain right from the outset of deformation. Individual domains rotate about TD and the predicted lattice orientation of all domains are shown in both Fig. 4 ⑦ and Fig. 6 (a_3). In the $N = 22$ domain model grain, as shown in Fig. 4 ⑦, 13 domains rotate 17.5° about +TD (▲) and 7 domains rotate 17° about −TD ($\triangledown$). Two domains remain oriented close to the initial crystal orientation (+). The predicted lattice rotations are consistent with the

experimental observations of Bauer et al. (1977), who observed band lattice rotations of 35° about ±TD at $\epsilon_{\text{vM}} = 0.92$. The predicted deformation band aligns with the rolling plane in agreement with the experimental observation of Heye and Sattler (1971).

Heye and Sattler (1971) have reported that E oriented copper single crystals undergo deformation banding during plane strain compression. The present model also predicts deformation banding in the E grain (high $\bar{\mu} = 18.93°$ and low $L = 1.04$). As seen from Fig. 5(a), out of the $N = 22$ domains, 9 domains rotate about +TD (▲) and the remaining 13 domains rotate about −TD (▽). The angle of both rotations is approximately 19°. Moreover, the model deformation bands align with the rolling plane. The predicted lattice rotation and band boundary orientation agrees with the experimental observation of Heye and Sattler (1971). Unlike in the NRC grain, banding in the model E grain initiates only at $\epsilon_{\text{vM}} = 0.15$.

The model cube oriented copper grain also deformation bands as indicated by $\bar{\mu} = 11.53°$ and $L = 1.02$. The lattice orientation of all the domains before and after deformation is given in Fig. 5(b). It is seen that the $N = 22$ domain model grain divides into 5 different bands, viz., B_1, B_2, B_3, B_4 and B_5 marked in Fig. 5(b). Lattice rotation of the original cube orientation about +RD gives band B_1 comprised of 7 domains. The −RD lattice rotation corresponds to band B_2 comprised of 9 domains. The lattice rotation about +TD and −TD give bands B_3 and B_4, respectively, comprised of 2 domains each. The remaining 2 domains comprising band B_5 undergo almost no lattice rotation. Deformation banding in the model grain initiates at $\epsilon_{\text{vM}} = 0.11$.

The above predictions agree with the experimental observations of Wróbel et al. (1994) that a cube oriented copper single crystal deformation bands. They report that up to a strain of $\epsilon_{\text{vM}} = 0.92$, i.e., 60% reduction, the lattice rotation about RD is significant and further deformation gives lattice rotation about TD also. Interestingly, rotation about RD is not reported in the literature on cube oriented aluminum single crystals (Akef and Driver, 1991; Wert et al., 1997; Liu and Hansen, 1998; Liu et al., 2000). In the present model for copper, tendencies

for lattice rotation about both RD and TD are observed. The former tendency, however, clearly dominates, in accord with observations in copper by Wróbel et al. (1994) .

5.1.3. Shear banding

According to the experimental literature, C oriented copper single crystals undergo intense shear localization (Grewen et al., 1977; Morii and Nakayama, 1981; Nakayama and Morii, 1982; Wagner et al., 1995; Jasienski et al., 1996). The model grain also undergoes shear banding, as indicated by the high value of $L = 9.95$. In the $N = 22$ domain model C grain at $\epsilon_{\mathrm{vM}} = 0.31$, 21 domains are oriented close to the initial lattice orientation $\Phi \approx 33^\circ$ and only one domain, which undergoes intense slip activity, is oriented at $\Phi = 14.6^\circ$. This compares well with the experimental observation of Jasienski et al. (1996), who report $13.3^\circ \leq \Phi \leq 19.5^\circ$ in the shear band and $\Phi \approx 35^\circ$ in the matrix, after plane strain compression to $\epsilon_{\mathrm{vM}} = 0.31$. The division of model grain into shear bands and matrix occurs at $\epsilon_{\mathrm{vM}} = 0.22$. The predicted shear band in the C-grain is inclined 45° to RD and parallel to TD, as stated in Sec. 2.5. This closely agrees with the experimental observations of Jasienski et al. (1996), who reported shear bands parallel to TD and inclined 42° with RD.

5.1.4. Applicability to other materials

The present results are based on hardening parameters that are specific to pure copper. Markedly different banding responses occur in other medium or high stacking fault energy f.c.c. metals and alloys. For example, unlike the copper C oriented grain, the aluminum C grain is known not to develop shear bands (Driver et al., 1994; Wagner et al., 1995; Godfrey et al., 1998); only microshear bands that do not propagate across the crystal have been reported. Similarly, although both copper and aluminum cube oriented single crystals have been observed to deformation band, the deformation bands have been reported to rotate about RD at rolling reductions $< 60\%$ (Wróbel et al., 1994) in copper, and about TD in aluminum in the same strain range (Liu et al., 1998),

as noted above.

5.2. Comparison with previous model predictions

The predicted banding results are now compared with results obtained from banding theories or crystal plasticity finite element method (CPFEM) simulations available in the literature.

The deformation banding criterion of Lee et al. (1993) and Lee et al. (1995) is based on minimizing the work of plastic deformation. This simple criterion, which neglects lattice rotation during grain deformation, predicts that S, G and C grains will not deformation band, and that the cube grain will deformation band. Despite its simplicity, predictions based on this criterion agree with experimental observations. The present model predictions agree with those of Lee et al. in the case of grains common to both studies: the small values of $\bar{\mu} = 1.2^\circ$ (S), $\bar{\mu} = 0.15^\circ$ (G) and $\bar{\mu} = 2.1^\circ$ (C) obtained from the present calculations indicate no deformation banding, while $\bar{\mu} = 11.53^\circ$ for the present cube model grain indicates deformation banding.

Raabe et al. (2002) have performed CPFEM simulations of plane strain compression of a generic f.c.c. material deforming by $\{111\}\langle 110\rangle$ slip. They predict homogeneous deformation in the G, S and C orientations, and banding in the B and NRC orientations. The predictions for the G, S and NRC orientations agree with the present results, while those for the B and C orientations disagree with experimental data noted in Sec. 5.1 above and with the present predictions. The absence of a sophisticated material point hardening scheme and the coarse finite element mesh used in the calculations of Raabe et al. (2002) may underlie these deviations.

The CPFEM results of Kanjarla et al. (2010) shows that the grain in a columnar f.c.c. multicrystal with initial orientation close to NRC forms deformation bands. The predicted results of the present model for NRC grains also shows the formation of deformation bands as discussed in the previous section. The banding pattern in the CPFEM study is, however, inhomogeneously distributed, a feature that cannot be captured by the present model.

A detailed set of shear band predictions for typical texture components (C, B, S, G and cube) has been given recently by Kuroda and Tvergaard (2007, Fig. 6b) Their predictions are based on both simplified analysis and CPFEM simulations. In agreement with their predictions, shear banding in predicted in the present model in the C grains, while no banding is predicted presently in the G grain. However, the orientation of the predicted shear bands in present study deviate from those predicted by them. Also, their model predicts shear banding in the B and S orientations, which are known experimentally not to band in copper and are predicted not to band by the present model.

The predictions of Kuroda and Tvergaard (2007) pertain to an aluminum alloy assumed to harden isotropically. The sub-structure based hardening law in the present model is more complex and specifically pertains to pure copper. Banding predictions are sensitive to material hardening as noted in Sec. 5.1.4; this may partly explain the deviations of the present predictions from those of Kuroda and Tvergaard (2007). Also, while Kuroda and Tvergaard (2007) assumed that shear band boundaries are immobile relative to the material, the present shear band boundaries are assumed mobile. This likely explains the differences in the shear band orientations predicted by Kuroda and Tvergaard (2007) and those predicted presently. Another cause for the disparate predictions may be the constraints imposed on the grain: while full constraints are imposed in the present work, Kuroda and Tvergaard (2007) relaxed two shear constraints.

5.3. Role of surrounding grains

The focus of this study has been deformation inhomogeneity at the length scale of the grain that arises from the intrinsic instability of the grain's lattice orientation. That grain deformation inhomogeneity may also result from the extrinsic influence of inter-grain interactions has been shown both experimentally (Ørsund et al., 1989) and by CPFEM simulations (Beaudoin et al., 1996). Large lattice rotations of the order of 25° have been reported in intrinsically stable brass oriented aluminum alloy grains in a polycrystal, which suggests that

even when the lattice orientation of a grain is intrinsically stable, the interaction of a grain with its neighbors in a polycrystal may produce bands (Ørsund et al., 1989). Likewise, G grains, which have been shown above to have an intrinsic tendency to deform homogeneously, develop deformation bands when they are a constituent part of a bicrystal (Raabe et al., 2002) or a polycrystal (Delannay et al., 2008). Finally, extrinsic factors may also modify the banding pattern in an intrinsically unstable grain (Kanjarla et al., 2010).

The effect of the extrinsic interactions on banding in a grain can be determined using an extension of the present model; this is, however, deferred to future work.

6. Conclusions

A 'stack of domains' model of a grain has been used to simulate plane strain deformation of model copper grains initially oriented along the standard copper type f.c.c. rolling texture fibers: α, β and τ. Model predictions are used to characterize the intrinsic nature of banding along these fibers and the resulting microtexture that develops. Banding predictions have been compared with experimental observations reported in the literature. Quantitative agreement of the predicted microtexture with experimental observations is obtained. This suggests that it is important for banding models (i) to sufficiently capture the actual hardness evolution of material points within the grain and (ii) to account for mobility or immobility of band boundaries.

Acknowledgments: We thank Prof. V. Parameswaran for encouragement and for comments that helped improve this manuscript. Pole figures were drawn using the `POLE` software developed by Dr. Carlos Tomé. Funding was provided by the Indira Gandhi Center for Atomic Research, Kalpakkam and by the Board of Research in Nuclear Sciences.

References

Akef, A., Driver, J. H., 1991. Orientation splitting of cube-oriented face-centered cubic crystals in plane strain compression. Mater. Sci. Eng., A 132, 245–255.

Anand, L., Kalidindi, S. R., 1993. The process of shear band formation in plane strain compression of fcc metals: Effects of crystallographic texture. Mech. Mater. 17 (2–3), 223–243.

Arul Kumar, M., Mahesh, S., 2012. Banding in single crystals during plastic deformation. Int. J. Plasticity 36, 15–33.

Arul Kumar, M., Mahesh, S., Parameswaran, V., 2011. A stack model of rate-independent polycrystals. Int. J. Plasticity 27 (6), 962–981.

Asaro, R. J., 1979. Geometrical effects in the inhomogeneous deformation of ductile single crystals. Acta Metall. 27 (3), 445–453.

Bauer, R. E., Mecking, H., Lucke, K., 1977. Textures of Copper single crystals after rolling at room temperature. Mater. Sci. Eng. 27 (2), 163–180.

Bay, B., Hansen, N., Kuhlmann-Wilsdorf, D., 1989. Deformation structures in lightly rolled pure aluminum. Mater. Sci. Eng. A 113, 385–397.

Beaudoin, A. J., Mecking, H., Kocks, U. F., 1996. Development of localized orientation gradients in fcc polycrystals. Phil. Mag. A 73 (6), 1503–1517.

Chin, G. Y., Wonsiewicz, B. C., 1969. Deformation banding and the stability $\langle 100\rangle$–$\langle 111\rangle$ fiber textures in FCC materials. Trans. AIME 245, 871–872.

Delannay, L., Melchior, M. A., Kanjarla, A. K., Van Houtte, P., Signorelli, J. W., 2008. CPFEM Investigation of the Effect of Grain Shape on the Planar Anisotropy and the Shear Banding of Textured Metal Sheets. John Wiley & Sons, Ch. 79, pp. 745–756.

Dillamore, I. L., Roberts, J. G., Bush, A. C., 1979. Occurrence of shear bands in heavily rolled cubic metals. Metal Science 13, 73–77.

Driver, J. H., Jensen, D. J., Hansen, N., 1994. Large strain deformation structures in aluminum crystals with rolling texture orientation. Acta Metall. Mater. 42 (9), 3105–3114.

Engler, O., Randle, V., 2010. Introduction to texture analysis. CRC press.

Godfrey, A., Jensen, D. J., Hansen, N., 1998. Slip pattern, microstructure and local crystallography in an aluminum single crystal of copper orientation $\{112\}\langle 111\rangle$. Acta Mater. 46 (3), 835–848.

Grewen, J., Noda, T., Sauer, D., 1977. Electron microscopic investigation of shear bands. Z. Metallkd. Bd. 68 (H. 4), 260–265.

Heye, W., Sattler, H. P., 1971. Bildung von deformationsbandern in gewaltzen kuper-einkristallen. Z. Metallkd. 62, 386–391.

Hill, R., 1961. Discontinuity relations in mechanics of solids. In: Sneddon, I. N., Hill, R. (Eds.), Prog. Solid Mech. Vol. 2. Interscience Publishers, New York, Ch. 6, pp. 247–278.

Hirsch, J., Lucke, K., 1988. Mechanism of deformation and development of rolling textures in polycrystalline FCC metals: I Description of rolling texture in homogeneous CuZn alloys. Acta Metall. 36 (11), 2863–2882.

Hosford, W. F., 1966. Plane-strain compression of aluminum crystals. Acta Metall. 14, 1085–1094.

Huang, C. X., Wang, K., Wu, S. D., Zhang, Z. F., Li, G. Y., Li, S. X., 2006. Deformation twinning in polycrystalline Copper at room temperature and low strain rate. Acta mater. 54 (3), 655–665.

Hughes, D. A., Hansen, N., 1997. High angle boundaries formed by grain subdivision mechanisms. Acta Mater. 45 (9), 3871–3886.

Jago, R., Hatherly, M., 1975. Deformation banding in rolled Copper crystals. Metal Science 9, 83–89.

Jasienski, Z., Baudin, T., Piatkowski, A., Penelle, R., 1996. Orientation changes inside shear bands occurring in channel-die compressed (112)[$\bar{1}\bar{1}$1] Copper single crystals. Scr. Mater. 35 (3), 297–403.

Kanjarla, A. K., Van Houtte, P., Delannay, L., 2010. Assessment of plastic heterogeneity in grain interaction models using crystal plasticity finite element method. Int. J. Plasticity 26, 1220–1233.

Kocks, U. F., Tomé, C. N., Wenk, H. R., 1998. Texture and anisotropy. Cambridge Univ. Press, Cambridge, U.K.

Korbel, A., Szczerba, M., 1982. Strain hardening of Copper single crystals at high strains and dynamical recovery process. Acta metall., 1961–1968.

Kuhlmann-Wilsdorf, D., 1999. Regular deformation bands (DBs) and the LEDS hypothesis. Acta Mater. 47 (6), 1697–1712.

Kulkarni, S. S., Starke Jr, E. A., Kuhlmann-Wilsdorf, D., 1998. Some observations on deformation banding and correlated microstructures of two aluminum alloys compressed at different temperatures and strain rates. Acta Mater. 46 (15), 5283–5301.

Kuroda, M., Tvergaard, V., 2007. Effects of texture on shear band formation in plane strain tension/compression and bending. Int. J. Plasticity 23 (2), 244 – 272.

Lee, C. S., Duggan, B. J., 1993. Deformation banding and copper-type rolling textures. Acta Metall. Mater. 41 (9), 2691–2699.

Lee, C. S., Duggan, B. J., Smallman, R. E., 1993. A theory of deformation banding in cold rolling. Acta Metall. Mater. 41 (8), 2265–2270.

Lee, C. S., Smallman, R. E., Duggan, B. J., 1995. A simplified criterion for deformation banding applied to deformation texture simulation. Scr. Metall. Mater. 33 (5), 727–733.

Liu, Q., Hansen, N., 1998. Macroscopic and microscopic subdivision of a cold-rolled aluminium single crystal of cubic orientation. Proc. R. Soc. London, Ser. A 454, 2555–2592.

Liu, Q., Jensen, D. J., Hansen, N., 1998. Effect of grain orientation on deformation structure in cold rolled polycrystalline aluminium. Acta Mater. 46 (16), 5819–5838.

Liu, Q., Wert, J., Hansen, N., 2000. Location dependent lattice rotation and shear strain in rolled aluminum single crystals of cube and Goss orientations. Acta Mater. 48, 4267–4279.

Mahesh, S., 2006. Deformation banding and shear banding in single crystals. Acta Mater. 54 (17), 4565–4574.

Mahesh, S., 2010. A binary tree based model for rate-independent polycrystals. Int. J. Plasticity 26 (1), 42–64.

Mahesh, S., 2012. Orientation preferences of extended sub-granular dislocation boundaries. Philos. Mag. 92 (18), 2286–2312.

Malin, A. S., Huber, J., Hatherly, M., 1981. The microstructure of rolled Copper single crystals. Z. Metallkd. Bd. 72 (5), 310–317.

Moakher, M., 2002. Means and averaging in the group of rotations. SIAM. J. Matrix Anal. Appl. 24 (1), 1–16.

Morii, K., Nakayama, Y., 1981. Shear bands in rolled Copper single crystals. Trans. JIM 22 (12), 857–864.

Nakayama, Y., Morii, K., 1982. Transmission electron microscopy of shear band formation in rolled Copper single crystal. Trans. JIM 23 (7), 422–431.

Ørsund, R., Hjelen, J., Nes, E., 1989. Local lattice curvature and deformation heterogeneities in heavily deformed aluminium. Scripta Metall 23 (7), 1193 – 1197.

Paul, H., Driver, J. H., 2008. The influence of shear bands on microtexture evolution in polycrystalline copper. Ceram. trans. 200, 765–774.

Paul, H., Driver, J. H., Jasienski, Z., 2002. Shear banding and recryatsllization nucleation in a Cu-2%Al alloy single crystal. Acta Mater. 50, 815–830.

Paul, H., Maurice, C., Driver, J. H., 2010. Microstructure and microtexture evolution during strain path changes of an initially stable Cu single crystal. Acta mater. 58 (8), 2799–2813.

Paul, H., Morawiec, A., Driver, J. H., Bouzy, E., 2009. On twinning and shear banding in a Cu8 at.% Al alloy plane strain compressed at 77K. Int. J. Plasticity 25, 1588–1608.

Raabe, D., Zhao, Z., Park, S. J., Roters, F., 2002. Theory of orientation gradients in plastically strained crystals. Acta Mater. 50 (2), 421–440.

Rezvanian, O., Zikry, M. A., Rajendran, A. M., 2006. Microstructural modeling of grain subdivision and large strain inhomogeneous deformation modes in f.c.c. crystalline materials. Mech. Mater. 38 (12), 1159–1169.

Roters, F., Eisenlohr, P., Hantcherli, L., Tjahjanto, D. D., Bieler, T. R., Raabe, D., 2010. Overview of constitutive laws, kinematics, homogenization and multiscale methods in crystal plasticity finite-element modeling: Theory, experiments, applications. Acta Mater. 58 (4), 1152–1211.

Si, L. Y., Lu, C., Huynh, N. N., Tieu, A. K., Liu, X. H., 2008. Simulation of rolling behaviour of cubic oriented Al single crystal with crystal plasticity FEM. J. Mater. Process. Technol. 201 (1–3), 79–84.

Taylor, G. I., 1938. Plastic strain in metals. J. Inst. Metals 62, 307.

Van Houtte, P., Sevillano, J. G., Aernoudt, E., 1979. Models for shear band formation in rolling and extrusion. Z. Metallkd. 70, 426–432.

Wagner, P., Engler, O., Lücke, K., 1995. Formation of Cu-type shear bands and their influence on deformation and texture of rolled FCC $\{112\}\langle 111\rangle$ single crystals. Acta Metall. Mater. 43 (10), 3799–3812.

Wert, J. A., 2002. Macroscopic crystal rotation patterns in rolled aluminium single crystals. Acta Mater. 50, 3125–3139.

Wert, J. A., Huang, X., 2003. Extended planar boundary inclinations in FCC single crystals and polycrystals subjected to plane strain deformation. Philos. Mag. 83 (8), 969–983.

Wert, J. W., Liu, Q., Hansen, N., 1997. Dislocation boundary formation in a cold-rolled cube-oriented al single crystal. Acta Mater. 45, 2565–2576.

Winther, G., Huang, X., 2007. Dislocation structures. part ii. slip system dependence. Philos. Mag. 87 (33), 5215–5235.

Wróbel, M., Dymek, S., Blicharski, M., 1996. The effect of strain path on microstructure and texture development in Copper single crystals with (110)[001] and (110)[1$\bar{1}$0] initial orientations. Scripta mater. 35 (3), 417–422.

Wróbel, M., Dymek, S., Blicharski, M., Gorczyca, S., 1988. The development of dislocation structure and texture in rolled Copper (001)[110] single crystals. Textures and Microstructures 10 (1), 67–75.

Wróbel, M., Dymek, S., Blicharski, M., Gorczyca, S., 1993. Shear band formation in the rolled metals. Arch. Metall. 38 (2), 195–203.

Wróbel, M., Dymek, S., Blicharski, M., Gorczyca, S., 1994. Dislocation microstructure and texture development in rolled Copper single crystals. Z. Metallkd. 85 (6), 415–425.

Wu, G. L., Godfrey, A., Winther, G., Juul Jensen, D., Liu, Q., 2011. Evolution of orientations and deformation structures within individual grains in cold rolled columnar grained nickel. Acta mater. 59, 5451–5461.